molecular pharmaceutics

ARTICLE

pubs.acs.org/molecularpharmaceutics

Mannosylated Dextran Derivatives Labeled with *fac*-$[M(CO)_3]^+$ (M = ^{99m}Tc, Re) for Specific Targeting of Sentinel Lymph Node

Maurício Morais,[†] Suresh Subramanian,[‡] Usha Pandey,[‡] Grace Samuel,[‡] Meera Venkatesh,[‡] Manuel Martins,[§] Sérgio Pereira,[§] João D. G. Correia,[†] and Isabel Santos*[,†]

[†]Unidade de Ciências Químicas e Radiofarmacêuticas, ITN, Estrada Nacional 10, 2686-953 Sacavém, Portugal

[‡]Radiopharmaceuticals Division, Bhabha Atomic Research Centre, Mumbai, India 400 085

[§]CICECO, Universidade de Aveiro, Portugal

Supporting Information

ABSTRACT: Despite being widely used in the clinical setting for sentinel lymph node detection (SLND), ^{99m}Tc-based colloids (e.g., ^{99m}Tc-human serum albumin colloids) present a set of properties that are far from ideal. Aiming to design novel compounds with improved biological properties, we describe herein the first class of fully characterized ^{99m}Tc(CO)$_3$-mannosylated dextran derivatives with adequate features for SLND. Dextran derivatives, containing the same number of pendant mannose units (13) and a variable number (*n*) of tridentate chelators (**9**, *n* = 1; **10**, *n* = 4, **11**, *n* = 12), have been synthesized and fully characterized. Radiolabeled polymers of the type *fac*-[^{99m}Tc(CO)$_3$(k^3-L)] (**12**, L = **9**, **13**, L = **10**, **14**, L = **11**) have been obtained quantitatively in high radiochemical purity (≥98%) upon reaction of the dextran derivatives with *fac*-[^{99m}Tc(CO)$_3$(H$_2$O)$_3$]$^+$. The highly stable compounds **13** and **14** were identified by comparing their HPLC chromatograms with the ones obtained for the corresponding rhenium surrogates *fac*-[Re(CO)$_3$(k^3-**10**)] (**13a**) and *fac*-[Re(CO)$_3$(k^3-**11**)] (**14a**), which have been characterized both at the chemical (NMR and IR spectroscopy, and HPLC) and physical level (DLS, AFM and LDV). Compounds **13a** and **14a** present a positive zeta potential (+ 7.1 mV, pH 7.4) and a hydrodynamic diameter in the range 8.4−8.7 nm. Scintigraphic imaging and biodistribution studies in Wistar rats have shown good accumulation in the sentinel node at 60 min postinjection (6.71 ± 2.35%, **13**; and 7.53 ± 0.69%, **14**), with significant retention up to 180 min. A clear delineation of the sentinel lymph node without significant washout to other regions was observed in the scintigraphic images. The popliteal extraction of 94.47 ± 2.45% for **14** at 1 h postinjection, as compared to 61.81 ± 2.4% for **13**, indicated that **14** is a very promising compound to be further explored as SLN imaging agent.

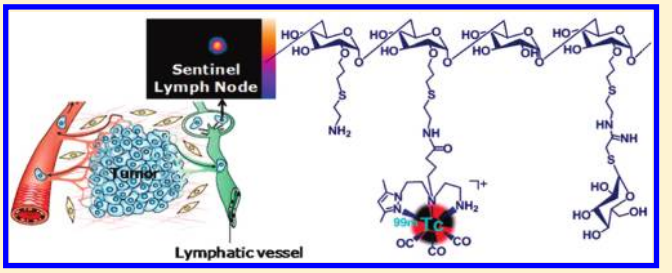

KEYWORDS: sentinel lymph node imaging, ^{99m}Tc-tricarbonyl, Re-tricarbonyl, dextran, mannose

INTRODUCTION

The sentinel lymph node (SLN) is the first lymph node that receives lymphatic drainage from a primary tumor, and the application of this concept to nuclear medicine is well established. An accurate identification and characterization of SLN is very important as it helps to decide the extension of surgery, the tumor staging, and the establishment of the most adequate therapy.[1−3]

Lymphoscintigraphy and sentinel node biopsy are the two major methods that widely govern SLN diagnosis.[1,4] Lymphoscintigraphy is a radionuclide-based technique for imaging regional lymph node drainage systems, providing functional and morphological information of the lymphatic network. This technique is typically performed by injecting a radiolabeled colloid and a blue dye. The radiotracer is used to determine the anatomical location of the node with a gamma probe and to guide the dissection. The blue dye is typically injected at the beginning of surgery to facilitate the visualization of the lymphatic drainage.[3,5] ^{99m}Tc-human serum albumin colloids (HSA) and filtered ^{99m}Tc-sulfur colloids (fTcSC) are in clinical use for lymphoscintigraphy, although not universally approved by the regulatory authorities, due to their nonideal properties.[5−7] From the clinical point of view, an ideal tracer must combine persistent retention in the SLN, low distal lymph node accumulation, fast clearance rate from the injection site, safe radiation exposure level, and lack of toxicity. The parameters that affect the biological properties of the tracers for SLN detection (SLND) are unclear, but it is considered that nature, size and surface characteristics of the nanoparticles may play a significant role.[5−8]

Mannose receptors, expressed by lymph node macrophages, have been considered attractive targets to design receptor-specific diagnostic agents for SLND.[9−13] Based on this principle,

Received: December 13, 2010
Accepted: February 7, 2011
Revised: January 31, 2011
Published: February 07, 2011

Scheme 1. Synthesis of 9−11[a]

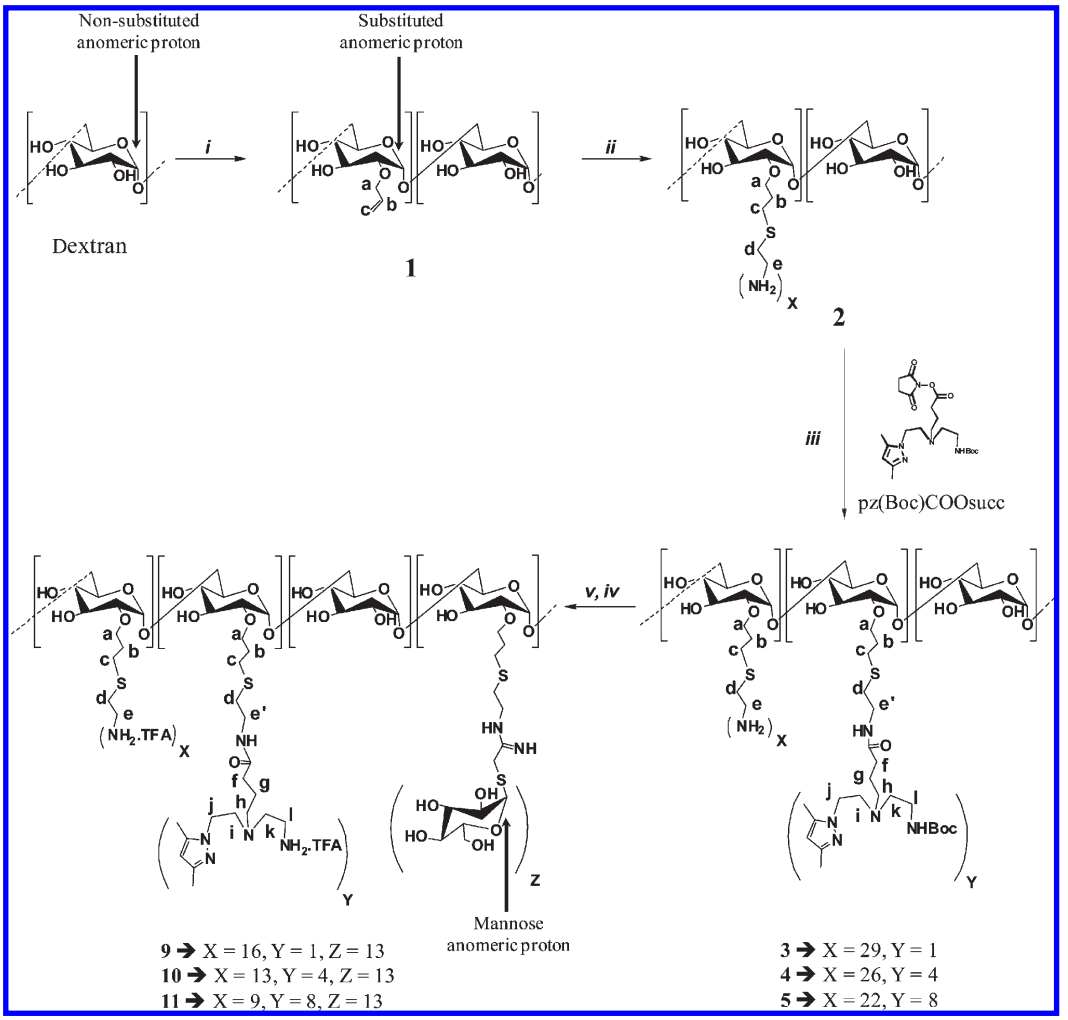

[a] (i) BrC_3H_5, NaOH (2.5 M), H_2O; (ii) $NH_2(CH_2)_2SH$, $(NH4)_2S_2O_8$, DMSO; (iii) pz(Boc)COOsucc, borate buffer 0.1 M, pH 9; (iv) IME-mannose, borate buffer 0.1 M, pH 9; (v) TFA/H_2O.

albumin and dextran functionalized with mannose units were synthesized and labeled with ^{99m}Tc.[14−16] The mannosylated ^{99m}Tc-diethylene triaminepentaacetic acid (DTPA)-labeled dextran, introduced by Vera et al., has shown the most promising *in vivo* behavior, being currently in clinical trials.[17] However, from the chemical and radiochemical point of view, DTPA cannot be considered an ideal bifunctional chelator to stabilize Tc. Indeed, the chemistry of this metal with DTPA is not well-defined, some controversy existing about the nature of the complex formed at the non carrier added (n.c.a.) level.[18] Therefore, further improvement is needed to prepare highly stable and chemically well-defined target-specific ^{99m}Tc complexes for SLND. Aiming to contribute to this purpose, and taking advantage of both the versatile ^{99m}Tc-tricarbonyl technology and superior coordination properties of the pyrazolyl-diamine (pz) chelator,[19−22] we decided to prepare the first mannosylated-dextran conjugates labeled with ^{99m}Tc-tricarbonyl for SLND.

Herein, we report on the synthesis and characterization of novel mannose−dextran conjugates loaded with a different number (1, 4, 8 units/mol of dextran) of pyrazolyl-diamine chelating units. The labeling of such nanocarriers with *fac*-$[M(CO)_3]^+$ (M = ^{99m}Tc, Re), their chemical and physical characterization, and biological evaluation for SLND will be also reported.

METHODS

Materials. Dextran (9,500−10,500 g/mol) and mannose were purchase from Sigma Aldrich. The Boc protected pyrazolyl-diamine chelator (pzBoc) and cyanomethyl-2,3,4,6-tetra-*O*-acetyl-1-β-mannopyranoside (CNM-thiomannose) were prepared according to described procedures.[22,23] All the other chemicals not specified were purchased from Aldrich. Na[^{99m}TcO4] was eluted from a ^{99}Mo/^{99m}Tc generator, using 0.9% saline. The IsoLink kit (Mallinckrodt-Covidien, Petten, Holland) was used to prepare *fac*-[^{99m}Tc$(CO)_3(H_2O)_3]^+$, and *fac*-[Re$(CO)_3(H_2O)_3$]Br was prepared as described.[19,24] ^{1}H and ^{11}C NMR spectra were recorded at room temperature on a Varian Unity 300 MHz spectrometer. ^{1}H and ^{13}C chemical shifts were referenced with the residual solvent resonance relative to tetramethylsilane. The spectra were assigned based on 2D experiments (^{1}H−^{1}H correlation spectroscopy, COSY). The assignment of the ^{1}H and ^{13}C NMR peaks has been made

as indicated in the reaction scheme, Scheme 1. Infrared spectra were recorded as KBr pellets on a Bruker Tensor 27 spectrometer.

HPLC Methods. The HPLC analysis was performed on Perkin-Elmer equipment coupled to a gamma (Berthold Lb 509) and to a UV/vis detector (Shimadzu SPD-10 AV or Perkin Helmer Lc 290). Analysis was done either by reversed-phase high performance liquid chromatography (RP-HPLC) or by size exclusion chromatography (SEC-HPLC). RP-HPLC: Supelco Discovery Bio Wide Pore C18 25 cm × 4.6 mm, 5 μm analytical column; flow, 1 mL/min; eluents, A, TFA 0.1% in H_2O; B, TFA 0.1% in CH_3CN. SEC-HPLC: Shodex OHpack SB-803 HQ analytical column; flow, 0.5 mL/min; eluent, ammonium acetate 0.5 M. Resolution of the column was calculated to be 0.76 ± 0.29. The wavelengths for UV detection were 220 and 254 nm for RP-HPLC and SEC-HPLC, respectively.

Instant Thin Layer Cromatography (ITLC). Analysis was performed using PALL Life Sciences (prod. 61886) or Gelman Sciences Inc. (prod. 51432) strips and three different eluent systems (A, B, C). Radioactivity detection was performed on a radio chromatographer (Berthold LB 2723) equipped with 20 mm diameter NaI(Tl) scintillation crystal.

System A: Methyl Ethyl Ketone (MEK). $[TcO_4]^-$ migrates in the front of the solvent (R_f = 1), while $[^{99m}Tc(CO)_3(H_2O)_3]^+$, radioactive nanoconjugates and colloidal species stay at the origin (R_f = 0).

System B: 5% HCl 6 N/MeOH. $[^{99m}Tc(CO)_3(H_2O)_3]^+$ and $[TcO_4]^-$ migrate in the front of the solvent (R_f = 1), while radioactive nanoconjugates and colloidal species stay at the origin (R_f = 0).

System C: C_5H_5N/AcOH/H_2O (3:5:1). Colloidal species stay at the origin (R_f = 0). $[^{99m}Tc(CO)_3(H_2O)_3]^+$, $[TcO_4]^-$ and radioactive nanoconjugates migrate in the front of the solvent (R_f = 1).

Synthesis of Dextran-allyl (1). Dextran-allyl was prepared according to a method described previously with some modifications.[25] Dextran (1.00 g, 0.10 mmol) in water (7.5 mL) and excess of allyl bromide (2.50 mL, 14.5 mmol) reacted for 6 h. After dialysis against water, the retentate was concentrated under reduced pressure and lyophilized, yielding dextran-allyl (**1**) as a white solid (0.98 g, 0.09 mmol, 87%, $MW_{calculated}$ = 11,164 g/mol).

^1H NMR (300 MHz, D_2O) δ_H: 5.93 (m, H^b), 5.29 (m, H^c), 5.02 (0.82 H, s broad, $H_{subst.anom.}$), 4.86 (1 H, s broad, 1H, $H_{anom.}$), 4.11 (d, H^a), 3.78−3.35 (m, dextran); ^{13}C NMR (75.3 MHz, D_2O) δ_C: 133.7 (C^b), 118.0 (C^c), 97.5 ($C_{anom.}$), 95.7 ($C_{subst.anom.}$), 78.2 (C^a), 73.2−65.3 (5C, dextran).

Synthesis of Dextran-amine (2). A solution of dextran-allyl (**1**) (0.61 g, 0.05 mmol) in dry DMSO (3 mL) reacted with aminoethanethiol (0.75 g, 6.60 mmol) and ammonium persulfate (0.1 g, 0.43 mmol) for 3 h at room temperature. The pH of the reaction mixture was adjusted to 4 with sodium hydroxide, and the volume of the mixture was double with sodium acetate buffer 0.02 M, pH 4. After dialysis against sodium acetate 0.02 M, pH 4 and water, the retentate was concentrated and lyophilized, yielding dextran-amine (**2**) as a white solid (0.668 g, 0.05 mmol, 92%, $MW_{calculated}$ = 13,320 g/mol).

^1H NMR (75.3 MHz, D_2O) δ_H: 5.05 (s broad, $H_{subst.anom.}$), 4.87 (s broad, $H_{anom.}$), 3.64 (d, H^a), 3.80−3.30 (m), 3.14 (t, H^d), 2.78 (t, H^e), 2.60 (s broad, H^c), 1.76 (s, H^b); ^{13}C NMR (75 MHz, D_2O) δ_C: 99.7 ($C_{anom.}$), 97.8 ($C_{subst.anom.}$), 81.3 (C^a), 75.3−67.4 (5C, dextran), 40.3 (C^e), 30.7 (C^d), 30.1 (C^c), 29.1 (C^b).

Table 1. Molar Ratios Used To Prepare Conjugates 3−5, Experimental Molar Ratios and Reaction Yields

	molar ratios pz/NH_2		
conjugates	used	obtained	reaction yield (%)
3	0.15	0.03 ± 0.01	96
4	0.25	0.15 ± 0.01	96
5	0.4	0.3 ± 0.01	94

Quantification of Amine Units on Dextran Backbone. The number of amine groups per mole of dextran was calculated on the basis of three determinations, using the following equation:[14]

$$\text{amine number/mol of dextran} = \frac{[NH_2]}{[\text{glucose}]} \times n \qquad \text{(I)}$$

where $[NH_2]$ = amine concentration determined by the trinitrobenzene sulfonate assay (TNBS), using cysteamine solutions as standard;[26] [glucose] = glucose concentration determined by the sulfuric acid−phenol colorimetric assay, using glucose as standard;[27] and n = average number of glucose units/mole of dextran.

For the trinitrobenzene sulfonic acid (TNBS) assay, cysteamine solutions (5−50 μg in 1.5 mL of H_2O) were diluted in borate buffer 0.2 M, pH 8 (1.5 mL) and TNBS 5% (0.02 mL) was added. The mixture was vortexed and, after standing for 15 min at room temperature, absorbance readings were taken at 420 nm. Based on the calibration curve obtained ($y = 0.1296x - 6.9 \times 10^{-2}$; $r^2 = 0.9909$), the amine concentration of **2** was determined to be 698 ± 0.61 μM, based on three determinations.

For the sulfuric acid−phenol assay, a 5% phenol solution in H_2O (0.5 mL) and concentrated H_2SO_4 (2.5 mL) were added to glucose solutions (5−50 μg in 0.5 mL of H_2O) and the mixture was vortexed. After standing for 30 min at room temperature, absorbance readings were taken at 490 nm. Based on the calibration curve obtained ($y = 0.1236x + 2.76 \times 10^{-2}$; r^2 = 0.9973), the glucose concentration per mole of dextran was found to be 1400 ± 5.9 μM, based on three determinations.

Synthesis of the Dextran-amine-[pyrazolyl-diamine-(Boc)]$_y$ (3, y = 1; 4, y = 4; 5, y = 8). *General Procedure.* The carboxylic acid of the Boc protected pyrazolyl-diamine chelator (pz(Boc)) was activated with *N,N'*-dicyclohexylcarbodiimide (DCC) and *N*-hydroxysuccinimide (NHS) in dry CH_2Cl_2. After reacting at room temperature for 18 h, the DCC−urea precipitate was removed by filtration and the filtrate was vacuum-dried, yielding the corresponding activated ester pz(Boc)COOsucc as a yellow pail oil. This ester was dissolved in CH_3CN and added to a solution of dextran-amine (**2**) in borate buffer 0.1 M, pH 9, using different pz(Boc)COOsucc/amine molar ratios (Table 1). After overnight reaction at room temperature, the mixture was dialyzed, first against borate buffer 0.02 M, pH 9, and finally against water.

3 *(y = 1).* pz(Boc) (0.03 g, 0.08 mmol) and NHS (0.011 g, 0.09 mmol) were suspended in dry CH_2Cl_2 (5 mL), and DCC (0.011 g, 0.09 mmol) was added in solid form. After reaction (18 h), the solvent was evaporated and the resulting activated ester pz(Boc)COOsucc was redissolved in CH_3CN (1 mL) and added to a solution of **2** (0.174 g, 0.01 mmol) in borate buffer 0.1 M, pH 9 (26 mL). The reaction mixture was dialyzed against borate buffer 0.02 M, pH 9 and water. The retentate was dried under vacuum, and the solid obtained was washed with chloroform and

methanol, yielding **3** as a white solid (0.17 g, 0.01 mmol, 96%, $MW_{calculated}$ = 13,580 g/mol)

4 *(y = 4).* pz(Boc) (0.059 g, 0.161 mmol) and NHS (0.022 g, 0.193 mmol) were suspended in dry CH_2Cl_2 (5 mL), and DCC (0.022 g, 0.193 mmol) was added in solid form. After reaction (18 h), the solvent was evaporated and the resulting activated ester pz(Boc)COOsucc was redissolved in 1 mL of CH_3CN and added to a solution of **2** (0.286 g, 0.022 mmol) in borate buffer 0.1 M, pH 9 (28 mL). After workup as indicated for **3**, compound **4** was obtained as a white solid (0.30 g, 0.02 mmol, 96%, $MW_{calculated}$ = 14,630 g/mol).

5 *(y = 8).* pz(Boc) (0.103 g, 0.278 mmol) and NHS (0.039 g, 0.33 mmol) were suspended in CH_2Cl_2 (5 mL) and DCC (0.134 g, 0.33 mmol) was added in solid form. After reaction (18 h), the solvent was evaporated and the resulting activated ester pz-(Boc)COOsucc was redissolved in 1 mL of CH_3CN and added to a solution **2** (0.300 g, 0.023 mmol) in borate buffer 0.1 M, pH 9 (30 mL). After workup as indicated for **3**, compound **5** was obtained as a white solid (0.341 g, 0.021 mmol, 94%, $MW_{calculated}$ = 16,030 g/mol).

As an example, the NMR data for the Boc protected compound **4** is presented ^{1}H NMR (300 MHz, D_2O) δ_H: 5.82 (s, H(4)pz), 5.03 (s, broad, $H_{subst.anom.}$), 4.85 (s, broad, $H_{anom.}$), 3.88−3.35 (m, dextran), 3.21 (s, broad), 2.99 (s, broad), 2.81 (s, broad), 2.56 (s, broad), 2.08 (s, Mepz), 1.98 (s, Mepz), 1.61 (s, broad), 1.31 (s, 9H, CH_3). ^{1}H NMR data for the Boc protected **3** and **5** are given in the Supporting Information.

Aliquots of **3**, **4** and **5** were treated with TFA, to remove the Boc protecting group, and the resulting compounds analyzed by ^{1}H NMR, to determine the number of pyrazolyl chelating units. All the spectra gave similar patterns, the main difference being related to the intensity ratio of the peaks due to methyl groups of the pyrazolyl ring (3,5-Me_2pz) and the ones due to the protons adjacent to the unsubstituted amines (H^e).

As an example, the NMR data obtained for **4**, after removing the Boc protecting group, is presented. ^{1}H NMR (300 MHz, D_2O) δ_H: 5.92 (s, H(4)pz), 4.96 (s, broad, $H_{subst.anom.}$), 4.85 (s, broad, $H_{anom.}$), 3.88−3.35 (m, dextran), 3.10 (t, H^d), 2.74 (t, H^e), 2.56 (s, broad), 2.27 (t, H^h), 2.21 (s, Mepz), 2.14 (s, Mepz), 1.85 (s, broad), 1.74 (s, H^b).

Synthesis of Dextran-amine-[pyrazolyl-diamine(Boc)]$_y$-mannose (6, *y* = 1; 7, *y* = 4; 8, *y* = 8). **6**: A solution of sodium methoxide (10.8 mg, 1 mL,) was added to a dry methanolic suspension of CNM-thiomannose (0.7 g in 16 mL of methanol). After 20 h at room temperature, the solvent was evaporated, affording a golden syrup that reacted with a solution of **3** (0.100 g, 0.007 mmol) in borate buffer 0.1 M, pH 9.0 (5 mL) for 20 h at room temperature. The reaction mixture was concentrated and dialyzed first against borate buffer 0.02 M, pH 9.0, and finally against water. The retentate was concentrated and lyophilized, yielding **6** as a pale yellow solid (0.093 g, 0.006 mmol, 75%, MW est. = 16,870 g/mol).

7: The compound was prepared as above, using conjugate **4** (0.11 g, 0.01 mmol) to yield **7** as a pale yellow solid (0.096 g, 0.005 mmol, 74%, $MW_{calculated}$ = 17,920 g/mol).

8: The compound was prepared as above, using conjugate **5** (0.20 g, 0.001 mmol) to yield **8** as a pale yellow solid (0.196 g, 0.01 mmol, 80%, $MW_{calculated}$ = 18,850 g/mol).

^{1}H NMR spectra of **6**−**8** have similar patterns, the main difference being related to the intensity ratio between some of the ^{1}H NMR peaks. As an example, the NMR data for **8** is presented. ^{1}H NMR (300 MHz, D_2O) δ_H: 5.85 (s, H(4)pz), 5.27 (d, $H_{anom.mannose}$), 5.01 (s, broad, $H_{anom.subst.}$), 4.82 (s, broad, $H_{anom.}$), 3.99 (s, broad), 3.78−3.35 (m, dextran), 2.99−2.76 (m), 2.59 (s, broad), 2.17 (s, Mepz), 2.07 (s, Mepz), 1.8 (s, broad), 1.31 (s, 9H, CH_3).

Synthesis of Dextran-amine-[pyrazolyl-diamine]$_y$-mannose (9, *y* = 1; 10, *y* = 4; 11, *y* = 8). The Boc protecting groups in **6**−**8** were removed with TFA/H_2O affording the final conjugates **9**−**11** in quantitative yield. The compounds were characterized by SEC-HPLC, NMR and IR spectroscopy.

Based on the intensity ratio between the mannose anomeric proton (H_{anom}, δ 5.22), the Me-pz (δ 2.14) and the protons adjacent to free amine of the dextran backbone (H^e, δ 2.74), the number of mannose units per mole of dextran was calculated to be 13 ± 1.

As an example, the NMR data for **10** is presented. ^{1}H NMR (300 MHz, D_2O) δ_H: 5.80 (s, H(4)pz), 5.22 (s,broad $H_{mannose\ anom.}$), 4.99 (s, broad, $H_{subst.anom.}$), 4.82 (s, broad, $H_{anom.}$), 4.39 (t, CH_2^j), 3.99 (s, broad), 3.74−3.35 (m, dextran), 3.10 (t, H^d), 2.74 (t, H^e), 2.52 (s, broad), 2.24 (t, H^h), 2.07 (s, Mepz), 1.98 (s, Mepz), 1.74 (s, broad, H^b), 1.46 (t, H^g). ^{13}C NMR (75.3 MHz, D_2O) δ_C: 176.4 (C═O), 165.9 (C═N), 162.8 (q, CF_3COO^-), 150.5 (C(3)pz), 143.7 (C(5)pz), 116.5 (q, CF_3COO^-), 107.4 (C(4)pz), 99.9 ($C_{anom.}$), 97.8 ($C_{subst.anom.}$), 86.9, 86.7, 82.4, 81.5 (C^a), 75.8−68.9 (m, 11$C_{dextran/mannose}$), 68.5, 67.4, 63.1, 62.8 (C^k), 54.5 (C^i), 52.3, 47.9 (C^j), 43.9 (C^l), 40.6 (C^e), 39.3, 35.2, 31.0, 30.8 (C^d), 30.3 (C^c), 29.6, 29.1 (C^b), 24.4 (C^g), 14.3 (Mepz), 12,3 (Mepz). For ^{1}H NMR data of **9** and **11** see the Supporting Information.

IR (KBr) (ν/cm^{-1}): ν (OH, br) 3418, ν (C═O, s) 1678, ν (C═O, s, dextran) 1643, 1384, 1261.

SEC-HPLC (λ = 254 nm): **9**, t_R = 16.8 min; **10**, t_R = 16.4 min; **11**, t_R = 15.6 min.

Synthesis of *fac*-[^{99m}Tc(CO)$_3$(L)]$^+$ (*fac*-[^{99m}Tc(CO)$_3$]-2, L = 2; 12, L = 9; 13, L = 10; 14, L = 11). The precursor *fac*-[^{99m}Tc(CO)$_3$(H_2O)$_3$]$^+$ was prepared using the Isolink kit (Covidien) and its radiochemical purity checked by RP-HPLC.

Compounds *fac*-[^{99m}Tc(CO)$_3$]-**2** and **12**−**14** were obtained by reacting the dextran derivatives **2** and **9**−**11** with *fac*-[^{99m}Tc(CO)$_3$(H_2O)$_3$]$^+$. Briefly, a solution of *fac*-[^{99m}Tc(CO)$_3$(H_2O)$_3$]$^+$ (1 mL) was added to a capped vial, previously flushed with N_2, containing **2** (5×10^{-5} M) and **9**−**11** (2.5×10^{-5} M). The mixture reacted at 100 °C for 30 min, and the radiochemical purity of **12**−**14** was checked by RP-HPLC, SEC-HPLC and ITLC.

Stability Studies in the Presence of Cysteine and Histidine. Aliquots of *fac*-[^{99m}Tc(CO)$_3$]-**2** and **12**−**14** (100 μL, 10^{-5} M) were added to a large molar excess (1:100) of cysteine or histidine solutions in PBS (900 μL, 10^{-3} M, pH 7.4). The samples were incubated at 37 °C and analyzed by RP-HPLC and ITLC after 2, 4, and 6 h of incubation. The results are summarized in Table 2.

Synthesis of *fac*-[Re(CO)$_3$(k^3-L)]$^+$ (13a, L = 10; 14a, L = 11). Complexes **13a** and **14a** were prepared by reacting *fac*-[Re(CO)$_3$(H_2O)$_3$]Br[24] with compounds **10** and **11** in H_2O, using a rhenium precursor/pz molar ratio of 4:1. After stirring at 50 °C for 16 h, the reaction mixtures were concentrated and dialyzed against water and the retentate was concentrated and lyophilized. The resulting pale yellow powder was washed with CH_2Cl_2 and methanol. The progress of these reactions was monitored by taking aliquots of the reaction mixture at several time points. The aliquots were dialyzed overnight, dried under reduced pressure and washed with chloroform and methanol, yielding a yellow solid that was analyzed by RP-HPLC and ^{1}H NMR spectroscopy (Figure 3). When

Table 2. *In Vitro* Stability of $^{99m}Tc(CO)_3$-2 and 12−14 in the Presence of Cysteine and Histidine, at Different Time Points

	activity bound to dextran derivatives (%)						
	cysteine				histidine		
compds	0 h	2 h	4 h	6 h	2 h	4 h	6 h
$^{99m}Tc(CO)_3$-**2**	78	69	49	nd[a]	61	50	nd
12	98	80	75	nd	89	85	nd
13	98	93	92	90	99	98	97
14	98	94	94	92	99	98	98

[a] Not determined.

complete, the reaction mixture was treated as referred above and the solids obtained were formulated as **13a** and **14a**, based on RP-HPLC, multinuclear NMR and IR spectroscopy.

The ^1H and ^{13}C NMR spectra of **13a** and **14a** present similar patterns, the main differences being the intensity ratio of some ^1H NMR peaks.

As an example, NMR and IR data for **13a** is presented. ^1H NMR (300 MHz, D_2O) δ_H: 6.1 (s, H(4)pz), 5.23 (d, $H_{mannose\ anom.}$), 4.98 (s, broad, $H_{subst.anom.dextran}$), 4.80 (s, broad, $H_{anom.}$), 4.39 (t, CH_2^j), 3.99 (s, broad), 3.74−3.35 (m, dextran), 3.10 (t, H^d), 2.71 (t, H^e), 2.52 (s, broad), 2.21 (s, Mepz), 2.12 (s, Mepz), 1.91 (t, H^g), 1.73 (s, broad, H^b). ^{13}C NMR (75.3 MHz, D_2O) δ_C: 195.2 (ReCO), 194.7 (ReCO), 193.1 (ReCO), 176.2 (C═O), 165.4 (C═N), 168.2 (q, CF3COO$^-$), 153.7 (C(3)pz), 144.3 (C(5)pz), 118.5 (q, CF_3COO^-), 114.6 (pz), 108.1 (C(4)pz), 97.9 ($C_{anom.}$), 96.1 ($C_{subst.anom.}$), 85.1, 79.5−65.7 (11C), 60.9, 42.0, 38.7, 33.8, 32.9, 30.7 (C^h), 30.9, 30.0, 27.3, 20.3, 15.5 (Mepz), 11.1 (Mepz). ^1H NMR and ^{13}C NMR data for **14a** are given in the Supporting Information.

IR (KBr) (ν/cm^{-1}): ν (O−H, br) 3397, ν (C−H, m) 2950, ν (C≡O, s) 2027, ν (C≡O, w) 1999, ν (C≡O, s) 1899, ν (C═O, s) 1678, ν (C═O, s, dextran) 1643, 1556, 1384.

RP-HPLC: **13a**, t_R = 12.6 min; **14a**, t_R = 12.6 min.

Physical Characterization. The hydrodynamic diameter and the zeta potential of dextran (9,500−10,500 g/mol), **2**, **10**, **11**, **13a**, and **14a** were determined in phosphate buffer 0.01 M, pH 7.4, by DLS using a ZetaSizer Nano ZS from Malvern. Particle size was measured at 25 °C with a 173° scattering angle. The surface charge was determined by electrophoretic mobility using laser doppler velocimetry (LDV) and zeta potential cells.

A Digital Instruments MultiMode scanning probe microscope (SPM) with a Nanoscope IIIA controller in tapping mode was used for the atomic force microscopy (AFM) measurements.

Biodistribution studies of *fac*-[$^{99m}Tc(CO)_3(k^3$-L)]$^+$ (13, L = 10; 14, L = 11). *In vivo* evaluation studies of **13** and **14** were carried out in a Wistar rat model. All animal experiments performed were in accordance with the guidelines of the institutional animal ethics committee. Female Wistar rats weighing 200−250 g were used in the experiment. The animals were first anesthetized by intraperitoneal injection of a mixture of xylazine (70 mg/kg) and ketamine (7 mg/kg). Boosters if subsequently required were given using ketamine alone. Then ∼50 μL of the ^{99m}Tc-labeled preparation (∼1.8 MBq containing ∼20 μg of the ligand) was injected subcutaneously in the footpad region. The area of injection was massaged gently with a strip of gauze pad for about 2 min to facilitate movement of the radiolabeled preparation from the injection site. The rejection criterion followed was observation of any bleeding at the site of injection or measurement of more than 0.5% of administered dose on the gauze pad. Postinjection (p.i.), the animals were kept in separate sets (n = 4 per set) for incubation periods of 15 min, 30 min, 60 min and 180 min under normal conditions, water provided ad libitum. Ten minutes prior to the end of each incubation period, the animals under anesthetized condition were given a subcutaneous administration of ∼50 μL of Patent Blue Dye (1% w/v in saline) in the same region as the labeled preparation. At the end of the incubation, the animals were sacrificed and the relevant organs and tissues, including the popliteal (which serves as the sentinel lymph node in this protocol) and secondary nodes, were excised for the determination of *in vivo* distribution of ^{99m}Tc activity. Radioactivity measurement was done on Integral Line flat-bed NaI(Tl) scintillation detector (Harshaw, USA). Activity retained in each organ/tissue was expressed as a percentage of the total injected dose (% ID). The results are summarized in Tables 4 and 5.

Popliteal extraction (PE) was calculated using the following equation:[14]

$$\text{PE}\ (\%) = \frac{\%\ \text{ID (popliteal)} - \%\ \text{ID (iliac)}}{\%\ \text{ID (popliteal)}} \times 100 \qquad \text{(II)}$$

Scintigraphic Imaging Studies of the Sentinel Lymph Node. Scintigraphic imaging was performed on the Millennium MPS medical imaging system (Wipro-GE Healthcare, India). Scintigraphic imaging studies for **13** and **14** were also performed in Wistar rat model. ∼37 MBq of the radiolabeled preparation (in 50 μL volume) was used for each imaging study (n = 3). The technique employed for anesthesia of animals and administration of **13** and **14** preparations was the same as for the above-referred biodistribution studies, excepting that blue dye was not injected in the imaging protocol. For the acquisition, the animals were placed with their dorsal side facing the camera. Planar static images were acquired at 10 min, 30 min, 60 min and 180 min p.i. using the Genie Acq Image Acquisition software (release 3.0). Acquisition parameters were as follows: matrix 256 × 256, zoom 1.33, 5 min acquisition time. The site of injection was masked with lead shielding during acquisition. Subsequent image processing was achieved with the Xeleris image processing software (version 1.0272). The image results are summarized in Figure 7.

RESULTS

Synthesis and Characterization of Dextran−Mannose−Pyrazolyl−Diamine Derivatives (9−11). Dextran−mannose conjugates loaded with one (**9**), four (**10**) and eight (**11**) pyrazolyl-diamine chelating units per mol of dextran were synthesized as depicted in Scheme 1.

The first step of the synthetic pathway involved the functionalization of dextran (MW: 9,500−10,500) with allyl groups, yielding compound **1**. Quantitative conversion of the allyl groups in **1** to amines yielded **2**. Reactions of **2** with pz(Boc)COOsucc, in different molar ratios, yielded the dextran derivatives **3**−**5** (Table 1).[22] A freshly prepared solution of 2-imino-2-methoxyethyl-1-thio-β-D-mannoside (IME-thiomannose) in borate buffer 0.1 M, pH 9, reacted with **3**−**5**, yielding the final dextran−mannose−pyrazolyl−diamine conjugates **9**−**11**, after Boc-deprotection with TFA/H_2O.

All dextran derivatives were analyzed by ^1H and/or ^{13}C NMR spectroscopy and, in the case of **2**, also by colorimetric assays.

Table 3. Group Density, Hydrodynamic Diameter (DLS), Zeta Potential and Calculated Molecular Weight of Dextran, 2, 10, 11, 13a and 14a

	group density (units/mol of dextran)					
compd	amine	pz	mannose	diam[a] (nm)	zeta potential[a] (mV)	MW calcd (g/mol)
dextran				4.3 ± 0.4	−9.9 ± 0.5	10,000
2	30			5.7 ± 0.5	7.7 ± 1.3	13,320
10	13	4	13	7.0 ± 0.3	6.6 ± 0.3	18,820
11	9	8	13	7.0 ± 0.7	7.3 ± 0.6	20,132
13a	13	4	13	8.4 ± 0.5	7.1 ± 0.7	19,904
14a	9	8	13	8.7 ± 0.3	7.1 ± 0.1	22,300

[a] Mean ± SD.

Table 4. Biodistribution Data for 13 in Wistar Rat Model at Different Time Points

	% ID/organ			
organ	15 min	30 min	1 h	3 h
liver	2.57 ± 1.17	4.06 ± 0.32	4.80 ± 1.03	6.49 ± 0.09
intestine	0.45 ± 0.10	0.59 ± 0.04	0.75 ± 0.06	0.95 ± 0.17
stomach	0.12 ± 0.03	0.18 ± 0.01	0.30 ± 0.05	0.52 ± 0.17
kidney	0.56 ± 0.19	0.82 ± 0.02	1.12 ± 0.27	1.20 ± 0.01
heart	0.06 ± 0.02	0.07 ± 0.00	0.06 ± 0.01	0.06 ± 0.02
lungs	0.48 ± 0.27	0.65 ± 0.01	0.83 ± 0.16	0.65 ± 0.04
spleen	0.12 ± 0.07	0.18 ± 0.08	0.32 ± 0.10	0.31 ± 0.04
blood (whole)	0.97 ± 0.34	1.47 ± 0.08	0.91 ± 0.02	0.96 ± 0.37
1st node	3.96 ± 0.87	7.43 ± 1.59	6.71 ± 2.35	5.98 ± 1.68
2nd node	0.83 ± 0.05	3.15 ± 0.83	2.59 ± 1.06	1.41 ± 0.50
site of inj	89.06 ± 0.28	80.93 ± 2.87	83.85 ± 1.37	79.50 ± 5.02
PE (%)	78.60 ± 3.39	57.85 ± 2.19	61.81 ± 2.42	76.65 ± 1.73

Table 5. Biodistribution Data for 14 in Wistar Rat Model at Different Time Points

	% ID/organ			
organ	15 min	30 min	1 h	3 h
liver	2.42 ± 0.47	3.74 ± 0.17	5.44 ± 1.06	6.84 ± 0.01
intestine	0.55 ± 0.07	1.21 ± 0.11	0.61 ± 0.57	1.28 ± 0.17
stomach	0.15 ± 0.03	0.27 ± 0.01	0.42 ± 0.01	0.74 ± 0.07
kidney	0.53 ± 0.02	0.94 ± 0.01	1.18 ± 0.20	1.67 ± 0.28
heart	0.04 ± 0.01	0.08 ± 0.02	0.09 ± 0.00	0.09 ± 0.03
lungs	0.32 ± 0.01	0.35 ± 0.05	0.43 ± 0.03	0.60 ± 0.07
spleen	0.12 ± 0.03	0.20 ± 0.10	0.25 ± 0.11	0.45 ± 0.04
blood (whole)	2.14 ± 0.01	2.86 ± 1.72	1.72 ± 0.81	1.55 ± 0.65
1st node	4.43 ± 0.27	4.31 ± 0.27	7.53 ± 0.69	5.21 ± 0.78
2nd node	1.09 ± 0.40	1.41 ± 0.28	0.41 ± 0.15	0.59 ± 0.14
site of inj	89.14 ± 2.09	87.24 ± 3.06	81.58 ± 0.35	81.13 ± 0.01
PE (%)	68.55 ± 1.35	76.27 ± 5.07	94.47 ± 2.45	87.81 ± 3.75

The ^{1}H NMR spectrum of **1** in D_2O has shown clearly two multiplets (δ 5.93, H^b; δ 5.29 H^c) and one doublet (δ 4.11 H^a) due to the protons of the allyl group. We could also clearly identify two broad singlets appearing at δ 5.02 and δ 4.86 assigned to the anomeric protons of the substituted and nonsubstituted glucose units, respectively. The intensity ratio of these two ^{1}H NMR peaks was used to evaluate the substitution degree, which was found to be 50 ± 5%, based on five different batches. Reaction of **1** with aminoethanethiol has been quantitative, as indicated by the absence of the three resonances due to the allyl groups in the ^{1}H NMR spectra of **2**. The ^{1}H NMR peaks assigned to the anomeric protons (substituted and unsubstituted glucose units) could be identified in these spectra, presenting chemical shifts comparable to those found in **1**. The amine density per mol of dextran in **2** was also estimated using TNBS and sulfuric acid−phenol colorimetric assays. The values found were 30 ± 3 amine groups per mole of dextran. As mentioned above, based on the NMR data, 50 ± 5% of all glucose units of the commercial dextran were functionalized with allyl groups and all these groups were transformed into amines. Considering that the dextran used has ca. 60 glucose units, it was found that ca. 30 of the glucose units have been derivatized with amines, a result which completely agrees with the colorimetric data. The number of pyrazolyl-diamine units in **3**−**5** was determined by ^{1}H NMR, after Boc deprotection of these conjugates. Based on the intensity of the ^{1}H NMR peaks attributed to methyl groups of the azolyl ring (δ 2.08, δ 1.98) and to the protons adjacent to free amine of the dextran backbone (δ 2.74, H^e), the number of pyrazolyl chelators in each compounds was found to be one (**3**), four (**4**) and eight (**5**) per mole of dextran. Then, the number of free amines was calculated to be 29 (**3**), 26 (**4**) and 22 (**5**).

The dextran−mannose−pyrazolyl−diamine conjugates **9**−**11** (overall yield >70% presented only one peak on the SEC-HPLC chromatograms, indicating a purity higher than 98%. The total number of mannose units per mole of dextran was calculated to be 13 ± 1, based on the intensity ratios of the peaks corresponding to the mannose anomeric proton (δ 5.22), 3,5-Me_2pz (δ 2.08) and protons adjacent to free amines (δ 2.74, H^e), easily assigned in the ^{1}H NMR spectra of **9**−**11**. As an illustrative example, we present in Figure 1 the ^{1}H NMR spectrum obtained for **10**, with the assignment of the most relevant peaks. NMR data for **3**, **5**, **9** and **11** are given in the Supporting Information.

Reactions of the Conjugates 9−11 with *fac*-[M(CO)$_3$(H$_2$O)$_3$]$^+$ (M = ^{99m}Tc, Re). The dextran−mannose−pyrazolyl−diamine derivatives **9**, **10** and **11** reacted with the precursors *fac*-$[M(CO)_3(H_2O)_3]^+$ (M = ^{99m}Tc or Re) leading to the corresponding metalated derivatives **12**−**14**, **13a** and **14a** (Scheme 2).

^{99m}Tc(CO)$_3$-mannosylated dextran derivatives (**12**−**14**) were analyzed by RP-HPLC and ITLC. The RP-HPLC chromatograms of **12** (t_R = 12.4 min), **13** (t_R = 12.6 min) and **14** (t_R = 12.6 min) presented only one species, and no free *fac*-[^{99m}Tc-(CO)$_3$(H$_2$O)$_3$] (t_R = 7.8 min) or any other radiochemical

dx.doi.org/10.1021/mp100425p |*Mol. Pharmaceutics* 2011, 8, 609–620

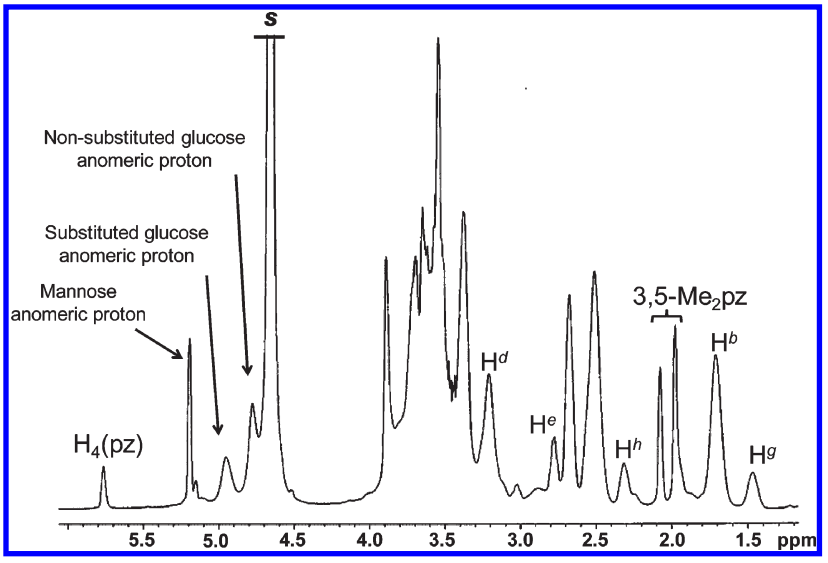

Figure 1. ^{1}H NMR spectrum of **10** in D_2O.

Scheme 2. Synthesis of *fac*-[M(CO)$_3$(k^3-L)] (M = ^{99m}Tc/Re: 12, L = 9; 13/13a, L = 10; 14/14a, L = 11)

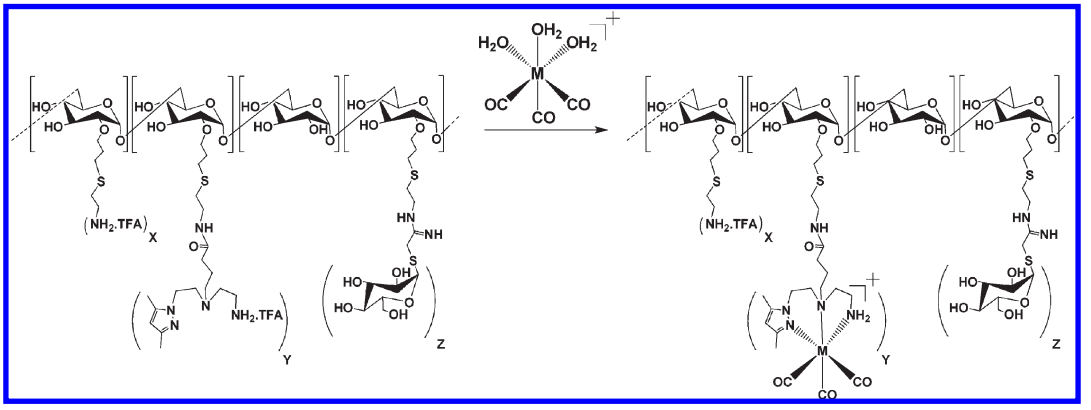

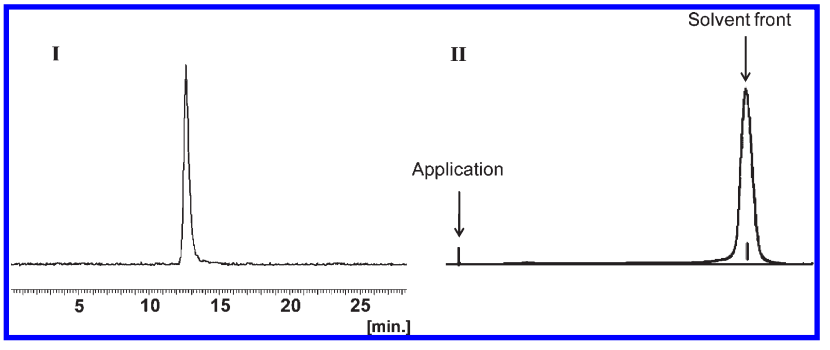

Figure 2. Radiochromatograms for **13**: (I) RP-HPLC chromatogram (t_R = 12.6 min); (II) ITLC (R_f = 1) using system C as eluent.

impurity could be detected. By ITLC it was also confirmed that **12**−**14** are formed with high radiochemical purity (>95%), as no $[TcO_4]^-$, *fac*-$[^{99m}Tc(CO)_3(H_2O)_3]^+$ or aggregates were detected. As an example, Figure 2 shows the RP-HPLC and ITLC chromatograms obtained for **13**.

Owing to the existence of donor atoms on **2**, with coordination affinity for *fac*-$[^{99m}Tc(CO)_3]^+$, we have also labeled directly this polymeric derivative with *fac*-$[^{99m}Tc(CO)_3(H_2O)_3]^+$. The resulting radioconjugate $^{99m}Tc(CO)_3$-**2** was obtained in 78% yield, due to the presence of some radiochemical impurities,

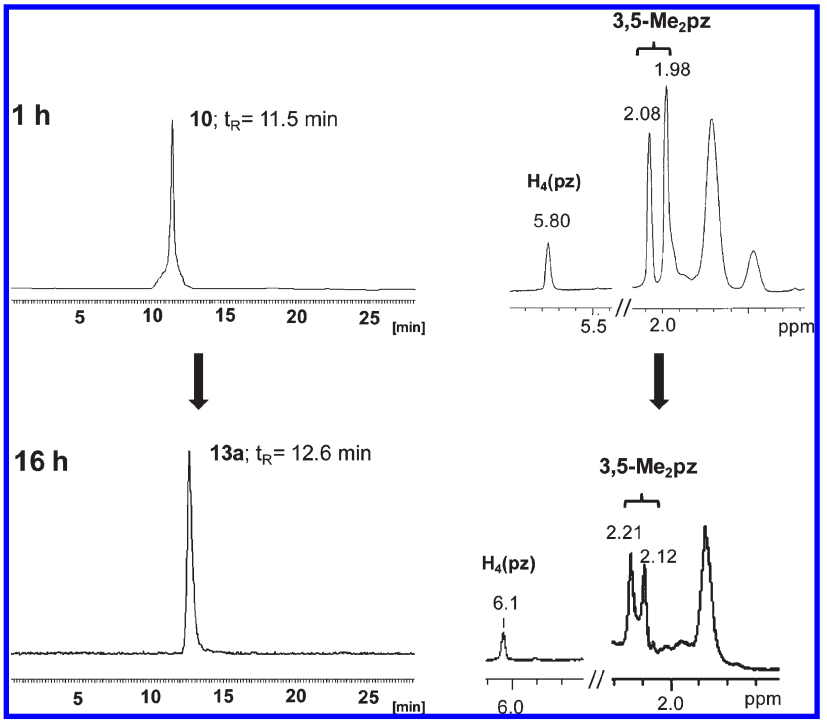

Figure 3. Progression of the reaction of *fac*-[Re(CO)$_3$(H$_2$O)$_3$]Br with **10**: RP-HPLC (λ = 220 nm) chromatograms and ^{1}H NMR data of the mixture after 1 h and 16 h of reagent addition.

which were identified by ITLC as aggregates and/or colloidal species.

^{99m}Tc(CO)$_3$-**2** and **12**−**14** were incubated with a large excess of cysteine and histidine to evaluate their *in vitro* stability toward transchelation. Table 2 summarizes the activity bound to the dextran derivatives at different time points.

^{99m}Tc(CO)$_3$-**2**, where no pyrazolyl-diamine chelating units are present, is obtained in relatively low yield (78%) and is not stable to transchelation. Compound **12**, with only one pyrazolyl-diamine chelator per mole of dextran, is obtained in almost quantitative yield but presents also a relatively low stability in the presence of cysteine and histidine. On the contrary, **13** and **14** are highly stable under the tested conditions, presenting in both cases high radiochemical purity (≥90%), even after long incubation times. Based on these results, compounds **13** and **14** were selected as the most promising radioactive compounds to pursue animal studies. Their characterization has been done by comparison of their HPLC chromatograms with the ones obtained for their rhenium mannosylated-dextran analogues, *fac*-[Re(CO)$_3$-(k^3-L)]$^+$ (**13a**, L = **10**; **14a**, L = **11**), synthesized as depicted in Scheme 2. The kinetics of these reactions were relatively slow, and their progress was monitored by RP-HPLC and ^{1}H NMR spectroscopy at different time points (1 h, 6 h and 16 h). As an example, Figure 3 shows the RP-HPLC chromatograms and ^{1}H NMR spectra for one of these reactions at 1 h and 16 h. From all the peaks appearing in the ^{1}H NMR spectra, we have only used the ones assigned to the pyrazolyl-diamine chelator, namely, to the H(4)pz and the 3,5-Me$_2$pz to evaluate the progress of the reaction. After 1 h, the H(4)pz and the 3,5-Me$_2$pz groups appear at δ 5.8, δ 2.08 and δ 1.98, respectively. The chemical shifts of these NMR peaks correspond to the free conjugate **10**, indicating that no metalation has taken place. By RP-HPLC it was also concluded that the peak at t_R = 11.5 min was due to **10**. After reacting 6 h, the ^{1}H NMR analysis showed that some metalation had taken place, but some uncoordinated ligand could still be detected (results not shown). Only after 16 h the reaction was complete, as indicated by the three ^{1}H NMR peaks at δ 6.1, δ 2.21 and δ 2.12 due to H(4)pz and 3,5-Me$_2$pz groups of **13a**. The chemical shift of these NMR peaks, compared to the values found in the free conjugate **10**, clearly confirmed the coordination of the metal to the pyrazolyl-diamine chelator. The RP-HPLC chromatograms also show only one peak for **13a**.

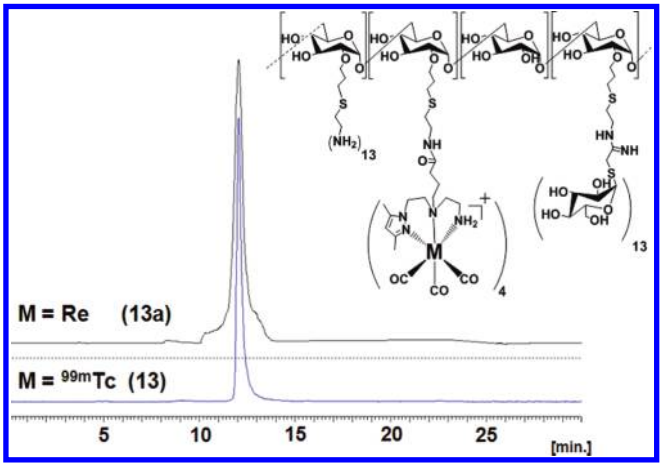

Figure 4. RP-HPLC chromatograms of **13** (γ-detection) and **13a** (λ = 220 nm).

In the ^{13}C NMR spectra of **13a** and **14a** the peaks assigned to the carbonyl groups of the *fac*-[Re(CO)$_3$]$^+$ core (**13a**, at δ 195.2, δ 194.7 and δ 193.1; **14a**, at δ 195.4, δ 194.9 and δ 193.2) could also be clearly seen in the expected range. The presence of such a core was also confirmed by the IR data obtained for **13a** and **14a** (ν(C≡O) strong bands in the range 2027−1998 cm^{-1}).[22]

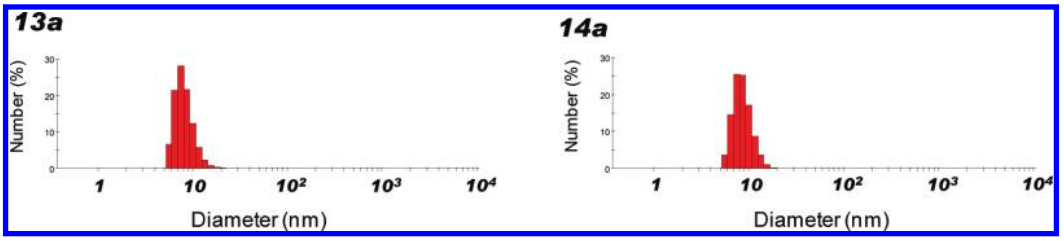

Figure 5. Hydrodynamic size of **13a** (8.4 ± 0.5 nm) and **14a** (8.7 ± 0.3 nm), determined by dynamic light scattering (detection angle of 173°).

A chromatographic comparative study (RP- and SEC-HPLC) of **13**/**13a** and **14**/**14a** allowed the characterization of the radioactive nanocompounds. As an example, Figure 4 displays the RP-HPLC chromatograms obtained for **13** (γ-detection) and **13a** (UV-detection). Identical results were obtained for **14**/**14a.**

Physical Characterization. The hydrodynamic diameter and the zeta potential of dextran, **2**, **10**, **11**, **13a** and **14a** were determined in phosphate buffer 0.01 M, pH 7.4, in order to mimic the labeling conditions. As an example, Figure 5 shows the size distribution histograms of **13a** and **14a**.

The final composition of the dextran derivatives, their physical parameters and the calculated molecular weight for each compound are summarized in Table 3.

The hydrodynamic diameter of the particles increases with the dextran backbone functionalization. However, the number of pyrazolyl-diamine chelating units (4 vs 8) does not affect significantly their size, as shown by the results obtained for **10** and **11**. Upon metalation of **10** and **11** a slight increase of the particles size was also found (**13a**, 8.4 ± 0.5 nm; **14a**, 8.7 ± 0.3 nm). Analysis of dextran, **13a** and **14a** by AFM, after dispersion on mica substrates, gave molecular diameters of ca. 4 nm (Figure 6A), 12 nm (Figure 6B), and 8−16 nm (Figure 6C) for dextran, **13a** and **14a**, respectively. AFM and DLS molecular measurements compare well for dextran and **13a**, the main difference being found for **14a**. The dispersion found for **14a** may indicate some aggregation during sample deposition.

Biodistribution Studies. Tables 4 and 5 show the *in vivo* distribution results after injection (p.i.) of **13** and **14** in Wistar rats, respectively.

Both radiocompounds show appreciable accumulation in the popliteal (sentinel) node. The highest radioactivity uptake in the sentinel node occurs between 30 and 60 min p.i., and a major portion of this is observed to be retained up to 180 min p.i. The popliteal extraction (PE), a parameter that predicts the suitability of a preparation as an agent for SLND, was determined according to eq II. The values found for **13** and **14**, at 1 h p.i, were 61.81 ± 2.42% and 94.47 ± 2.45%, respectively. Figure 7 displays the scintigraphic images of **13** (Figure 7A) and **14** (Figure 7B), showing a clear delineation of the sentinel node. In the case of **14** (Figure 7B), a greater degree of specific retention in the sentinel node is observed, with minimal spread to other regions.

■ DISCUSSION

^{99m}Tc-labeled mannosylated macromolecules like albumin and dextran of different molecular weights have been explored for SLND. For the dextran derivatives it was found that particles with size in the range 7−10 nm could be trapped, in a saturable mode, by the sentinel node.[15,16] Among them, mannosylated dextran labeled with Tc, using DTPA as a bifunctional chelating agent (Lymphoseek), was the most studied and the most promising for *in vivo* application. However, the chemical structure of technetium complexes with DTPA is not well-defined, and its chemical characterization has been the subject of many investigations and speculation at the macroscopic and n.c.a. level in the past few years.[18] Thus, taking into account that the real chemical structure of ^{99m}Tc-DTPA is unknown, there is interest on preparing fully characterized compounds with high radiochemical purity and specific activity, and adequate biological properties for SLND. Previously, we have introduced several pyrazolyl-based bifunctional chelators suitable for the stabilization of the core *fac*-$[M(CO)_3]^+$ (M = ^{99m}Tc, Re) and for the quantitative labeling of several biomolecules.[21,22] Profiting from these results, we decided to expand this technology to the synthesis of the first dextran−mannose derivatives containing one (**9**), four (**10**) and eight (**11**) pyrazolyl-diamine chelating units. These nanoconjugates, obtained in good overall yields (>70%), were quantitatively labeled with *fac*-$[^{99m}Tc(CO)_3]^+$, leading to the nanocomplexes **12**−**14**. The significant difference in labeling yields found for **12**−**14** (>95%) and $^{99m}Tc(CO)_3$-**2** (78%) clearly highlights the importance of the presence of those chelating units on the dextran backbone. Moreover, the number of these units seems also to be crucial for the kinetic inertness of the radioactive nanocompounds, as shown by the high stability of **13** and **14** compared to **12**. Most probably, when the number of pyrazoly rings is low, as in the case of **12**, the $^{99m}Tc(CO)_3$ binds to dextran through the pyrazolyl chelator but also through other coordinating groups existing in the dextran backbone. When this happens the radioactive nanocompound is not stable to transchelation, as shown for the species $^{99m}Tc(CO)_3$-**2**, where no chelators are present.

Due to the high labeling yields and stability, compounds **13** and **14** were selected for further biological studies.

Before such studies, **13** and **14** were chemically characterized at the macroscopic level by comparing their RP-HPLC chromatograms with the ones obtained for the rhenium analogues **13a** and **14a**, used as surrogates. These surrogates, formulated as *fac*-$[Re(CO)_3(k^3\text{-}L)]$ (**13a**, L = 10, **14a**, L = **11**), based on multinuclear NMR, HPLC and IR spectroscopy, were synthesized by reacting **10** and **11** with the precursor *fac*-$[Re(CO)_3(H_2O)_3]^+$. Additionally, **13a** and **14a** and the respective precursors (**10** and **11**) were physically characterized by DLS, AFM and LDV. The hydrodynamic diameters determined by DLS and AFM are of the same order of magnitude, and the values found showed an increase of the particle size due to both dextran functionalization and metalation. Taking into account the hydrodynamic diameter found for **10** (7.0 ± 0.3 nm), **11** (7.0 ± 0.7 nm), **13a** (8.4 ± 0.5 nm) and **14a** (8.7 ± 0.3 nm), the radioactive compounds **13** and **14**, used for biological studies, certainly have a hydrodynamic diameter in the range 7−9 nm. The hydrodynamic diameters of **10** and **11** are similar to those found for DTPA-mannosyl-dextran (7.1 ± 0.9 nm) and MAG_3-mannosyl-dextran (5.5 ±

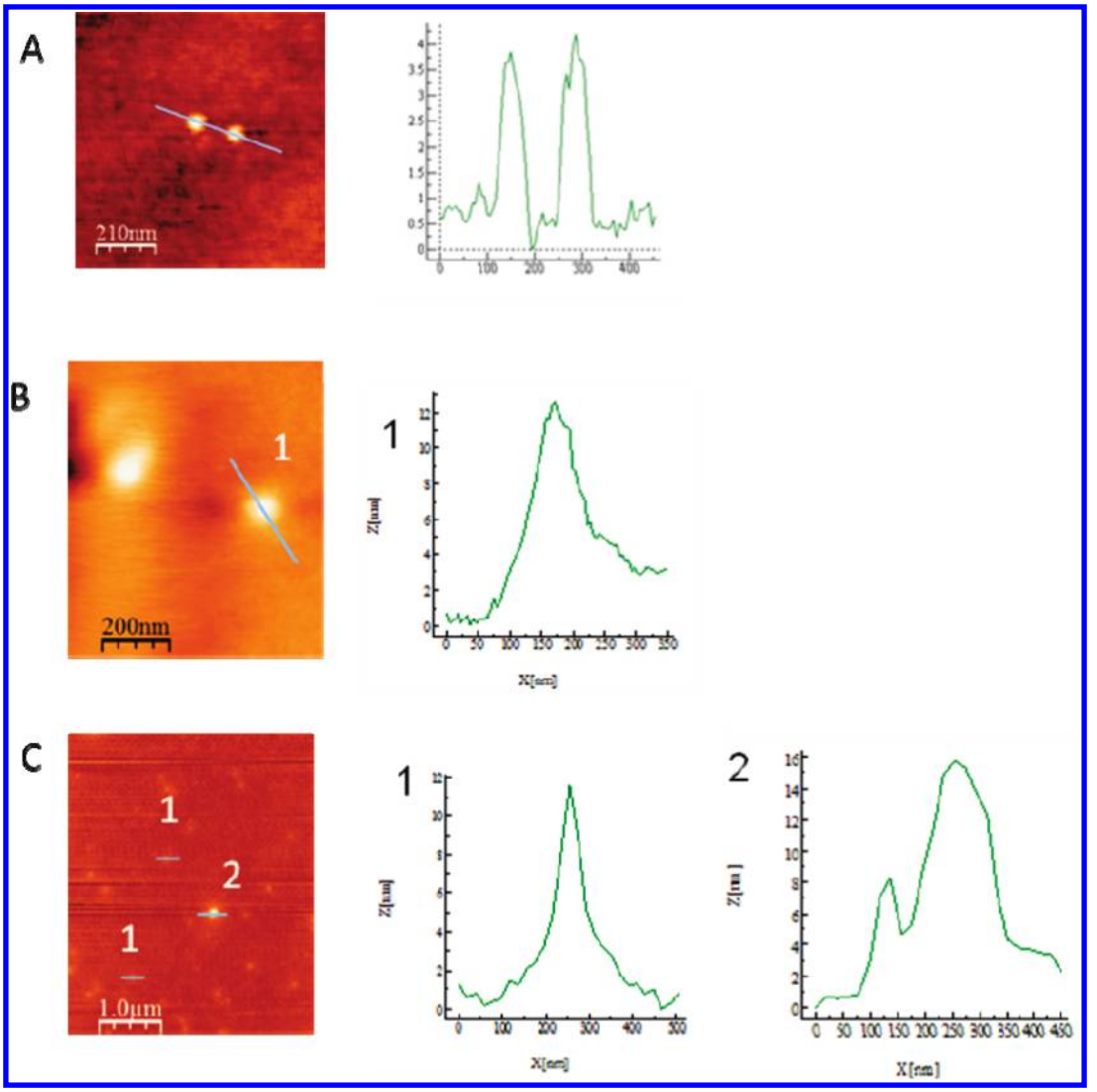

Figure 6. Height-scaled atomic force microscopy images and corresponding line profiles of dextran (A); **13a** (B); **14a** (C).

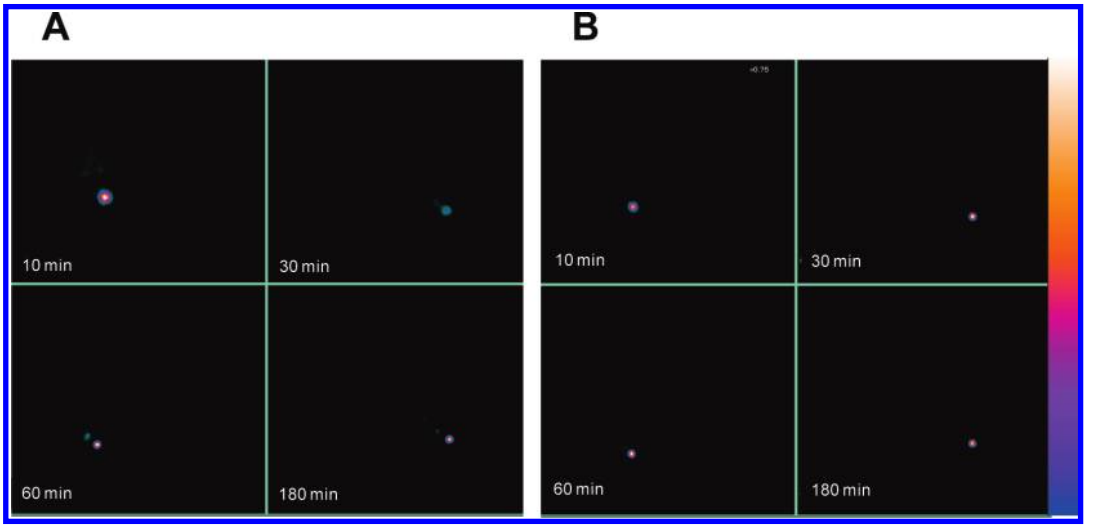

Figure 7. Scintigraphic images of Wistar rats injected with **13** (A) and **14** (B) at different time points.

2.4 nm), and much smaller than the radiopharmaceuticals in clinical use (80−100 nm).[5,14,15] As far as we are aware, no examples of mannosylated dextran derivatives have been synthesized and characterized at the macroscopic level, **13a** and **14a** being the first examples.

Zeta potential measurements indicated a negative charge for dextran (−9.9 ± 0.5 mV), which changed drastically upon functionalization with amines (**2**, +7.7 ± 1.3 mV). Our studies also indicated that further functionalization of **2** did not affect the charge of the nonmetalated (**10**, +6.6 ± 0.3 mV; **11**, +7.3 ± 0.6 mV) and metalated final nanocompounds (**13a**, +7.1 ± 0.7 mV; **14a**, +7.1 ± 0.1 mV). To the best of our knowledge, from all the nanocompounds studied for SLND, only the charge of ^{99m}Tc-MAG_3-mannosyl-dextran was determined by electrophoresis (negative overall charge).

The biodistribution results (Tables 4 and 5) and the scintigraphic images (Figure 7) of **13** and **14** have shown an appreciable accumulation in the popliteal (sentinel) node, the highest radioactivity uptake occurring between 30 and 60 min p.i. with a major portion of this retained up to 180 min p.i. The scintigraphic images for **13** and **14** clearly agree with the biodistribution pattern, as both show a clear delineation of the sentinel node and a great specific retention, mainly for **14**. For **13** some spread to the liver was observed. All biological data taken together renders **14** as a very favorable radiotracer for SLN imaging.

Our biological data cannot be directly compared with other nanotracers explored for SLND, namely, filtered ^{99m}Tc-sulfur colloid, ^{99m}Tc-DTPA-mannosyl-dextran (Lymphoseek), and ^{99m}Tc-HYNIC-NMA-tricine$_2$, as these compounds were evaluated in different animal models.[14,16] However, if we consider the PE parameter, **14** presents a value (1 h p.i.: 94.47 ± 2.47%) much higher than filtered ^{99m}Tc-sulfur colloid (78.8 ± 6.5%), and comparable to Lymphoseek (90.1 ± 10.7%) and ^{99m}Tc-HYNIC-NMA-tricine$_2$ (92.93 ± 5.08%).[14,16] The clearance from the injection site of **13** (83.85 ± 1.37%) and **14** (81.58 ± 0.35%) is comparable to that found for ^{99m}Tc-sulfur colloid (70.4 ± 11.0%) and slightly lower than for ^{99m}Tc-HYNIC-NMA-tricine$_2$ (67.57 ± 8.29%) and Lymphoseek (52.6 ± 10.5%), at 1 h p.i.[14,16] The charge of **13** and **14** may explain the moderate clearance from the injection site. In fact, **13** and **14** are positively charged, which may promote electrostactic interactions with the polyanionic glycosaminoglycans or other negatively charged species present in the interstitial space.[28] However, the high specific activity of the ^{99m}Tc-tricarbonyl complexes may also contribute to such behavior. Further studies on specific activity/injection site clearance are underway.

CONCLUSIONS

Aiming at the design of innovative radiotracers for SLN detection, we have introduced the first class of fully characterized ^{99m}Tc(CO)$_3$-mannosylated dextran derivatives with adequate biological features for SLN detection.

Several dextran derivatives (**9**−**11**), containing the same number of pendant mannose moieties (13 units) and a variable number of tridentate chelators (1 unit, **9**; 4 units, **10**; 12 units, **11**) have been synthesized and characterized. The radioactive nanocompounds of the type *fac*-[^{99m}Tc(CO)$_3$(k^3-L)] (**12**, L = **9**, **13**, L = **10**, **14**, L = **11**) were prepared quantitatively in high radiochemical purity (≥98%) and specific activity. Unlike **12**, the nanotracers **13** and **14** displayed very high *in vitro* stability, and have been chosen for biological studies. **13** and **14** were identified/characterized by comparing their chromatographic behavior with that of the corresponding rhenium surrogates **13a** and **14a**, which have been synthesized and characterized at both the chemical (NMR and IR spectroscopy, and HPLC) and physical levels (DLS, AFM and LDV). Scintigraphic imaging and biodistribution studies with **13** and **14** have shown good accumulation in the sentinel node at 60 min postinjection (6.71 ± 2.35% and 7.53 ± 0.69%, respectively), with significant retention up to 180 min. A clear delineation of the sentinel lymph node without significant washout to other regions was observed in the scintigraphic images. The higher PE of **14** compared to **13** highlights the superior biological properties of **14** to be further explored as SLN imaging agent.

Despite being evaluated in different animal models, the PE value found for **14** is higher than that found for fTcSC (78.8 ± 6.5%), routinely used for SLND, and comparable to the PE of Lymphoseek (90.1 ± 10.7%), which emerged as a promising radiotracer for SLND in recent clinical trials.

ASSOCIATED CONTENT

Supporting Information. ^{1}H NMR spectra of **3**, **5**, **9**, and **11**, ^{13}C NMR spectra of **14a**, and SEC-HPLC chromatograms of **10** and **11**. This material is available free of charge via the Internet at http://pubs.acs.org.

AUTHOR INFORMATION

Corresponding Author

*Instituto Tecnológico e Nuclear, Unidade de Ciências Químicas e Radiofarmacêuticas, Estrada Nacional, 10, 2686-953 Sacavém, Portugal. E-mail: isantos@itn.pt. Phone: +351219946201. Fax: 351 21 994 6185.

ACKNOWLEDGMENT

This work is part of the Coordinated Research Project (CRP) on the "Development of ^{99m}Tc radiopharmaceuticals for sentinel node detection and cancer diagnosis" of the IAEA, which is acknowledged. The authors also wish to thank John J. Zaknun and Ambi M. R. Pillai from the NA department of the IAEA, Vienna, for their active role in this CRP. Roberto Pasqualini is also acknowledged for fruitful scientific discussions. M.M. acknowledges FCT for a PhD grant (SFRH/BD/48066/2008).

REFERENCES

(1) Jain, R.; Dandekar, P.; Patravale, V. Diagnostic nanocarriers for sentinel lymph node imaging. *J. Controlled Release* **2009**, *138*, 90–102.

(2) Jeong, J. M.; Hong, M. K.; Kim, Y. J.; Lee, J.; Kang, J. H.; Lee, D. S.; Chung, J.; Lee, M. C. Development of 99mTc-mannosyl human serum albumin (^{99m}Tc-MSA) as a novel receptor binding agent for sentinel lymph node imaging. *Nucl. Med. Commun.* **2004**, *12*, 1211–1217.

(3) Scolyer, R. A.; Murali, R.; Satzger, I.; Thompson, J. F. The detection and significance of melanoma micrometastases in sentinel nodes. *Surg. Oncol.* **2008**, *17*, 165–174.

(4) Sharma, R.; Wendt, J. A.; Rasmussen, J. C.; Adams, K. E.; Marshall, M. V.; Muraca, E. M. New horizons for imaging lymphatic function. *Ann. N.Y. Acad. Sci.* **2008**, *1131*, 13–36.

(5) Wilhelm, A. J.; Mijnhout, S.; Franssen, E. J. F. Radiopharmaceuticals in sentinel lymph node detection: an overview. *Eur. J. Nucl. Med.* **1999**, 36–42.

(6) Eshima, D.; Fauconnier, T.; Eshima, L.; Thornback, J. R. Radiopharmaceuticals for lymphoscintigraphy: Including dosimetry and radiation considerations. *Semin. Nucl. Med.* **2000**, *1*, 25–32.

(7) Hoh, C. K.; Wallace, A. M.; Vera, D. K. Preclinical studies of ^{99m}Tc-DTPA-mannosyl-dextran. *Nucl. Med. Biol.* **2003**, *30*, 457–464.

(8) Jinno, H.; Kubo, A. Sentinel lymph node biopsy in breast cancer using technetium-99m tin. *Biomed. Pharmacother.* **2002**, *56*, 213–216.

(9) Liu, Y.; Chirino, A. J.; Misulovin, Z.; Leteux, C.; Nussenzweig, M. C.; Bjorkman, P. J. Crystal Structure of the Cysteine-rich Domain of Mannose Receptor Complex with sulphated Carbohydrate Ligand. *J. Exp. Med.* **2000**, *191*, 1105–1115.

(10) Ponpipom, M. M.; Bugianesi, R. L.; Robbins, J. C.; Doebber, T. W.; Shen, T. Y. Cell-specific ligands for selective drug delivery to tissue and organs. *J. Med. Chem.* **1981**, *24*, 1388–1395.

(11) Robbins, J. C.; Lam, M. H.; Tripp, C. S.; Bugianesi, R. L.; Ponpipom, M. M.; Shen, T. Y. Synthetic glicopeptides substrates for receptor-mediated endocytosis by macrophages. *Proc. Natl. Acad. Sci. U. S.A.* **1981**, *78*, 7294–7298.

(12) Liu, Y.; Chirino, A. J.; Misulovin, Z.; Leteux, C.; Nussenzweig, M. C.; Bjorkman, P. J. Crystal Structure of the Cysteine-rich Domain of Mannose Receptor Complex with sulphated Carbohydrate Ligand. *J. Exp. Med.* **2000**, *191*, 1105–1115.

(13) Higuchi, Y.; Oka, M.; Kawakami, S.; Hashida, M. Mannosylated semiconductor quantum dots for the labeling of macrophages. *J. Controlled Release* **2008**, *125*, 131–136.

(14) Vera, D. R.; Wallace, A. M.; Hoh, C. K.; Mattrey, R. F. A synthetic macromolcule for sentinel node detection: ^{99m}Tc-DTPA-Mannosyl-Dextran. *J. Nucl. Med.* **2001**, *42*, 951–959.

(15) Vera, D. R.; Wallace, A. M.; Hoh, C. K. [^{99m}Tc]−MAG_3-Mannosyl-Dextran: a receptor-binding radiopharmaceutical for sentinel node detection. *J. Nucl. Med.* **2001**, *28*, 493–498.

(16) Takagi, K.; Uehara, T.; Kaneko, E.; Nakayama, M; Koizumi, M.; Endo, K.; Arano, Y. ^{99m}Tc-labeled mannosyl-neoglycoalbumin for sentinel lymph node identification. *Nucl. Med. Biol.* **2004**, *31*, 893–900.

(17) Wallace, A. M.; Hoh, C. K.; Limmer, K. K.; Darrah, D. D.; Schulties, G.; Vera, D. R. Sentinel lymph node accumulation of Lymphoseek and Tc-99m sulfur colloid using a "2-day" protocol. *Nucl. Med. Biol.* **2009**, *36*, 687–692.

(18) Liu, G.; Hnatowich, D. J. Labeling Biomolecules with Radiorhenium - a Review of the Bifunctional Chelators. *Anticancer Agents Med Chem.* **2007**, *7*, 367–377.

(19) Alberto, R.; Ortner, K.; Wheatley, N.; Schibli, R.; Schubiger, A. Synthesis and properties of boranocarbonate: A convenient in situ CO source for aqueous preparation of fac-[^{99m}Tc$(H_2O)_3(CO)_3]^+$. *J. Am. Chem. Soc.* **2001**, *123*, 3135–3136.

(20) Alberto, R. The particular role of radiopharmacy within bioorganometallic chemistry. *J. Organomet. Chem.* **2007**, *692*, 1179–1186.

(21) Correia, J. D. G.; Paulo, A.; Santos, I. Re and Tc complexes with pyrazolyl-containing chelators: from coordination chemistry to target-specific delivery of radioactivity. *Curr. Radiopharm.* **2009**, *2*, 277–294.

(22) Alves, S.; Paulo, A.; Correia, J. D. G.; Gano, L.; Smith, C. J.; Hoffman, T. J.; Santos, I. Pyrazolyl derivatives as bifunctional chelators for labeling tumor-seeking peptides with the fac-$[M(CO)_3]^+$ Moiety (M) = ^{99m}Tc, Re): synthesis, characterization, and biological behaviour. *Bioconjugate Chem.* **2005**, *16*, 438–449.

(23) Lee, Y. C.; Stowell, C. P.; Krantz, M. J. 2-imino-2-methoxylethyl-1-thioglycosides: new reagents for attaching sugars to proteins. *Biochemistry* **1976**, *15*, 3956–3963.

(24) Lazarova, N.; James, S.; Babich, J.; Zubieta, J. A convenient synthesis, chemical characterization and reactivity of $[Re(CO)_3(H_2O)_3]$Br: the crystal and molcular structure of $[Re(CO)_3(CH_3CN)_2Br]$. *Inorg. Chem. Commun.* **2004**, *7*, 1023–1026.

(25) Holmberg, A.; Meurling, L. Preparation of sulfhydrylborane-dextran conjugates for boron neutron capture therapy. *Bioconjugate Chem.* **1993**, *4*, 570–573.

(26) Cayot, P.; Tainturier, G. The quantification of protein amino groups by the trinitrobenzenesulfonic acid method: a re-examination. *Anal. Biochem.* **1997**, *249*, 184–200.

(27) Rao, P.; Pattabiraman, T. N. Reevaluation of the phenol-sulfuric acid reaction for the estimation of hexoses and pentoses. *Anal. Chem.* **1989**, *181*, 18–22.

(28) Wiig, H; Kolmannskog, O.; Tenstad, O.; Bert, J. L. Effect of charge on interstitial distribution of albumin in rat dermis in vitro. *J. Physiol.* **2003**, *2*, 505–514.